Progress In Electromagnetics Research C, Vol. 85, 221–233, 2018

Design and Study of a Mechanical Flux-Varying PM Machine with Auto-Rotary PMs

Xiping Liu, Zhixuan Zhang*, Yufeng Liu, and Shaowen Cai

Abstract—By combining the theory of mechanical flux-adjusting with the advantages of an interior permanent magnet synchronous machine (PMSM), a new type of auto-rotary PMs mechanical flux-varying PM machine (ARPMMFVPMM) is creatively proposed in this paper. The operation principle and mechanical flux-adjusting mechanism were deeply investigated. The relationship between deformation of spring and auto-rotary angle of gear against speed was obtained by Automatic Dynamic Analysis of Mechanical System (ADAMS). Meanwhile, the electromagnetic characteristics of the machine were numerically analyzed by Finite Element Analysis (FEA). The simulation results show that the auto-rotary of cylindrical PMs is realized by the centrifugal force of mechanical device, and the range of speed regulation is expanded by adjusting the magnetic field distribution.

1. INTRODUCTION

With the development of rare earth permanent magnetic materials and electronic power devices, PMSM has been widely studied and applied recently. Especially for the rare earth PMSM, which generates excitation magnetic field using a high-performance rare earth permanent magnetic material, the operation efficiency and power factor are greatly improved [1–3]. However, there is also a significant shortcoming, which is the air-gap magnetic field of the PM machine, and it is difficult to regulate. In the application field of the generator, the output voltage of generator will fluctuate when the speed or the load changes [4]. In the application field of the motor, the limited speed range and low efficiency will appear when running at high speed. The shortcoming limits wide range of applications of PMSM [5, 6]. Therefore, the mode of field regulation is one of the most advanced research methods of PM machine to provide relevant theoretical basic and technical support for the application of PM machine, such as regulated power generation and constant power speed drive.

Variable flux permanent magnet synchronous machine (VFPMSM) is a special motor with variable air gap magnetic field. The change of magnetic flux can increase the starting torque when it runs at low speed or extend the speed range when it works at high speed [7]. The structures and principles of various VFPMSMs have been proposed [8–12]. Compared with the traditional PMSM, the VFPMSM with adjustable air gap magnetic field could satisfy the development of automotive industry, wide power generation and ship driving. The method of flux-adjusting for VFPMSM can be divided into three types: flux-adjustment directly [13–15], hybrid-excited by combination of PM and DC current [16–18] and mechanical adjustment [19–22]. First, direct flux-adjustment machine. This method is generally applicable to PMSM with variable speed drive and memory motor. The magnetic field produced by the continuous or instantaneous negative d-axis current will directly weaken the permanent magnet magnetic field, which achieves the purpose of flux-weakening. Second, hybrid-excited machine, namely, the hybrid of DC excitation and permanent magnet. By adjusting the size and direction of DC current, the purpose of changing the air gap magnetic field is achieved. Third, flux-adjusting mechanism machine.

Received 24 March 2018, Accepted 10 July 2018, Scheduled 24 July 2018
* Corresponding author: Zhixuan Zhang (1439687811@qq.com).
The authors are with the School of Electrical and Automation, Jiangxi University of Science and Technology, Ganzhou, China.

A regulated movement is generated by additional mechanical device, in which the air-gap magnetic field is varied by changing the relative position of stator and rotor, the size of magnetic leakage or the length of air gap.

Therefore, based on the advantages of compact structure, high efficiency and flexible adjustment of a PM machine with a flux-adjusting device, this paper presents a new type of ARPMMFVPMM, and its operation principle and magnetic adjustment mechanism are deeply studied. The change law of the rotation angle of the gear and the deformation length of the spring are analyzed by ADAMS. The electromagnetic characteristics are obtained by FEA. Combining the analysis of mechanical dynamics with electromagnetic characteristics, the characteristics of flux-adjusting are obtained, which provide a theoretical basis for the application of this machine in the field of new energy vehicle drive and wind power generation.

2. MODELING

2.1. The Structure of the Machine

The IPMSM mainly includes a rotor core, a stator core, winding and PMs, as shown in Figure 1. The armature winding adopts single layer and distributed winding with short pitch. It is helpful for eliminating the back EMF harmonics and improving the winding factor. The proposed rotor structure is composed of a number of NdFeB PMs arranged as rectangle shape and cylindrical shape. The cylindrical shape PMs have a matching slot hole beyond the rotor core part and is connected with mechanical flux-adjusting device through a connecting rod. Magnetic bridges are used in the middle and both sides of each layer of PMs to reduce magnetic flux leakage and improve the utilization of PMs. Compared with the IPMSM with single-layer PMs, the IPMSM with double-layer PMs can increase the difference of

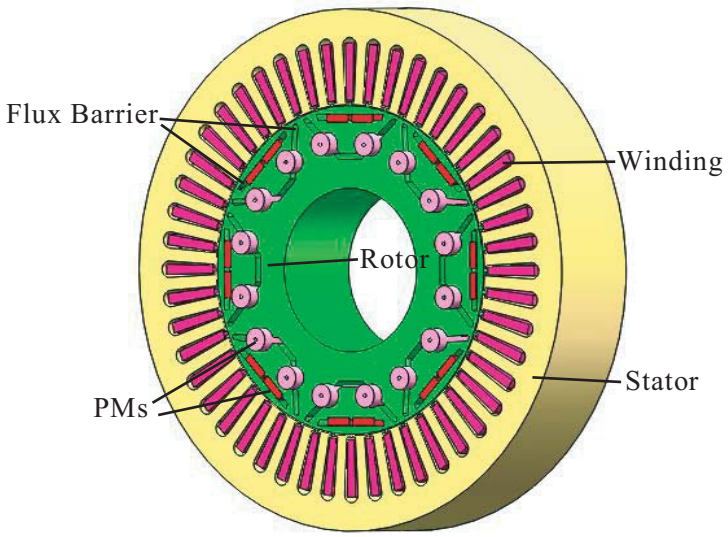

Figure 1. Structure of IPMSM.

Table 1. Partial parameters of machine.

Item	Value	Item	Value
rated power, kw	6.5	outer radius of stator, mm	255
rated voltage, v	380	Inner radius of rotor, mm	160.4
rotor pole number/stator slot number	8/48	number of conductors per slot	20
rated torque, nm	20.69	wire diameter, mm	0.65
rated speed, rpm	3000	winding connection	Wye

d-axis and q-axis inductances, improve the output torque and the distribution of efficiency. The partial parameters of machine are set as shown in Table 1.

2.2. The Structure of the Mechanical Device

The structure of the mechanical flux-adjusting device is shown in Figure 2, which mainly includes a disc, eight slide blocks, sixteen gears and connecting rods. The device is installed on the outside of the machine, connected by rotating the shaft and connecting rod. The rotating disc is used to place the slide blocks and gears, and the connecting rod is used to regulate the angle of PMs. Meanwhile, there are sliding chutes and connecting rod slots in the disc, which can make sliding block rectilinear moving and gear auto-rotating, respectively. The sliding block is connected with the disc by spring. The other end of the spring is connected with a raised ring of the disc, and the ring has slots. The sliding block is the driving source of mechanical flux-adjusting device, which makes full use of centrifugal force to drive the gear, so the linear motion of the sliding block is converted into a rotational motion of the gear. The cylindrical PMs in the rotor are rotated by the connecting rod, which realize the synchronous adjustment of the magnetic field with the change of speed. The structure is reliable, avoiding extra copper loss, and maintaining or improving efficiency in the process. The overall three-dimensional explosion diagram of the machine is shown in Figure 3.

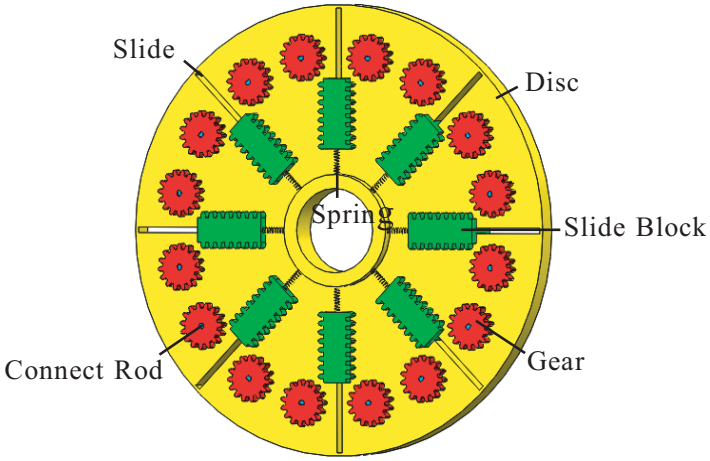

Figure 2. Structure of mechanical flux-adjusting device.

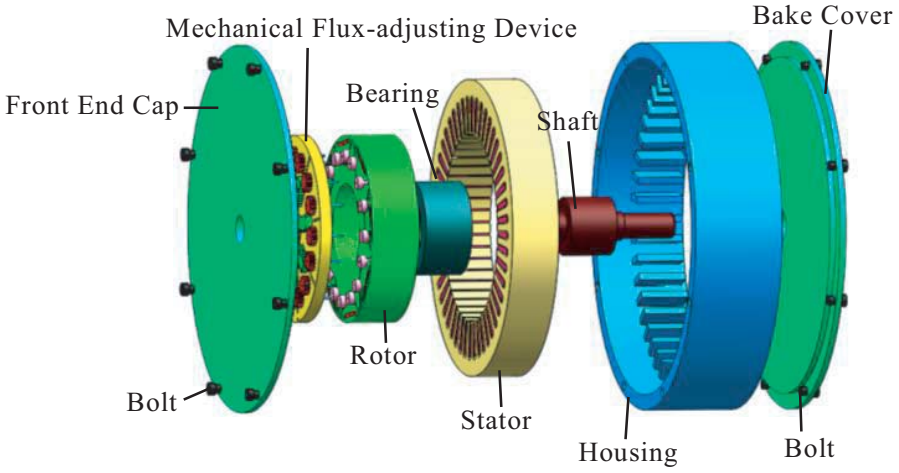

Figure 3. Three-dimensional explosion diagram.

3. OPERATION PRINCIPLE OF ARPMMFVPMM

The operation principle of ARPMMFVPMM is making the radial centrifugal force convert into the tangential force, and the tangential force makes the cylindrical PMs rotated centering on itself. After the PMs are rotated, the magnetization direction of the PMs is changed, and the distribution of air gap magnetic field of the machine is also changed.

3.1. The Principle of Mechanical Flux-Adjusting Device

There are three operation states of the machine, i.e., below the base speed, base speed and above the base speed, as shown in Figure 4. Under ideal conditions, the friction between the slider, the surface of the gear and the disc is ignored. The sliding block is only affected by spring force and centrifugal force. The force balance can finally be reached, and the contact with the gear is elastic contact.

(1) Below the base speed. When the machine runs at a constant speed below the base speed, the slider is subjected to the tension of the spring and the centrifugal force produced by circumferential rotation. The tension of spring is equal to the size of the centrifugal force, and the direction is opposite at this point. As shown in Figure 4(a), the sliding block is not in contact with the gear. There is no tangential driving force to the gear, and the maximum air gap flux density is obtained.

(2) Base speed. When the machine starts to accelerate below the base speed, the speed of sliding block also increases, then the centrifugal force is greater than the spring tension, and the sliding block moves linearly outwardly along the chute. The spring is forced to elongate and contacted between gear and sliding block at the base speed, as shown in Figure 4(b).

(3) Above the base speed. When the machine exceeds the base speed, the block drives the gear to rotate, and the gear drives the cylindrical PMs to spin through the connecting rod. The gear on the left side of sliding block is rotated counterclockwise and the gear on the right side rotated clockwise. At this time the position of the slider is marked with black, as shown in Figure 4(c). When the machine begins to decelerate from above the base speed to below the base speed, the spring force is greater than the centrifugal force, so the sliding block begins to make linear movement along the chute to the inside, and the rotation direction of the gear is opposite to that of acceleration. When the speed is reduced to under base speed, the sliding block is not in contact with the gear, and the PMs are rotated to the initial position. The movement of the sliding block and gear when decelerating is shown with blue marks in Figure 4(c).

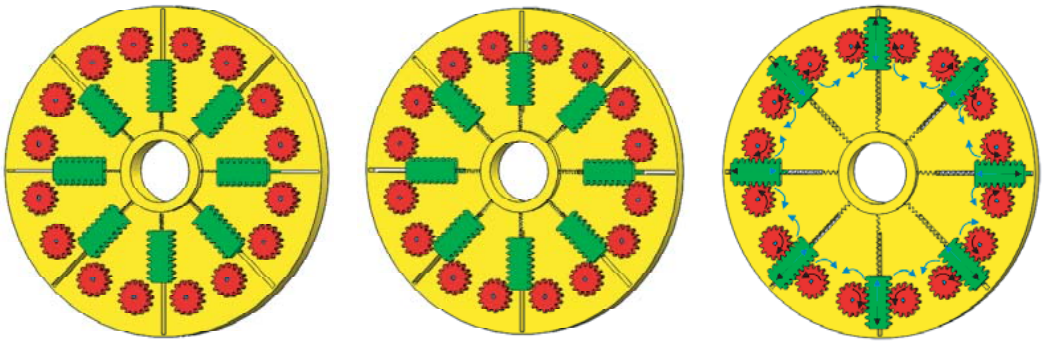

Figure 4. The principle of mechanical flux-adjusting device. (a) Below the base speed. (b) Base speed. (c) Above the base speed.

3.2. The Operation Principle of IPMSM

The operation principle of IPMSM is adjusting the direction of the magnetization of the interior cylindrical PMs. When the machine runs below the base speed, the magnetization direction of the

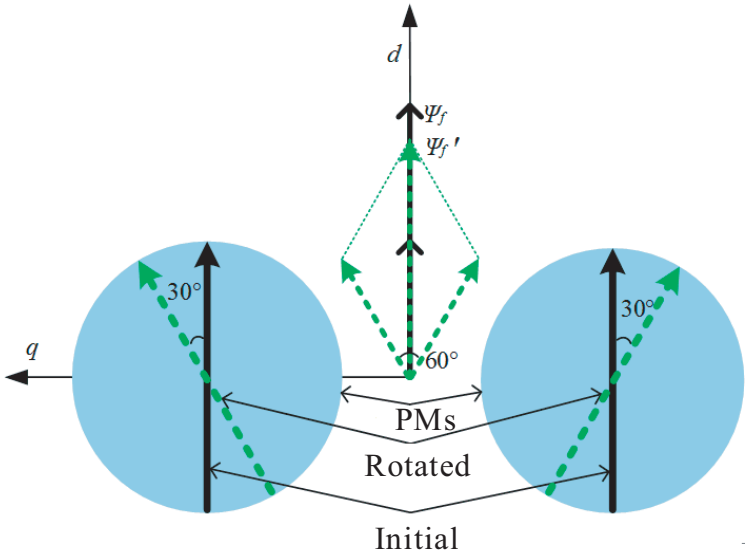

Figure 5. The operation principle of ARPMMFVPMM.

PMs is radial. Then through the action of mechanical flux-adjusting device, the left cylindrical PMs are rotated counterclockwise, and the right PMs are rotated clockwise. The PMs on both sides have the same rotation angle, and the direction of the magnetization synthesized does not change, while its vector synthesis is reduced. The operation principle of IPMSM is shown in Figure 5. Below the base speed, the two cylindrical PMs have the same direction of magnetization, and the vector synthesis of flux linkage is double that provided by one side of the PMs. Above the base speed, when the PMs rotate an angle, such as 30 deg, the composite PM flux linkage is $\sqrt{3}/2$ of basic speed, which achieves the effect of d-axis demagnetization.

According to the operation principle, the transformation of voltage worked by mechanical flux-adjusting device can be rewritten as Equation (1).

$$\begin{cases} u_d = R_a i_d + \cos\theta \dfrac{d\lambda_d}{d_t} - \sin\theta\omega_r\lambda_q \\ u_q = R_a i_q + \sin\theta \dfrac{d\lambda_q}{d_t} + \cos\theta\omega_r\lambda_d \end{cases}, \tag{1}$$

where θ is the self-rotation angle of cylindrical PMs.

The stator armature current at no-load is zero, then the voltage vector equation can be simply written as Equation (2).

$$\begin{cases} u_d = \cos\theta \dfrac{d\lambda_d}{d_t} - \sin\theta\omega_r\lambda_q \\ u_q = \sin\theta \dfrac{d\lambda_q}{d_t} + \cos\theta\omega_r\lambda_d \end{cases}, \tag{2}$$

4. THE MODEL OF VIRTUAL PROTOTYPE

For the ARPMMFVPMM, the key to changing the magnetic field is the centrifugal movement of sliding block when mechanical flux-adjusting device rotates synchronously. In order to analyze the relationship between the mechanism of flux-adjusting and the motion of mechanical device, it is necessary to analyze the mechanical dynamics characteristic.

Figure 6 shows a simplified virtual prototype model of mechanical flux-adjusting device. It consists of sliding blocks, gears and a disc. The default material of mechanical device is steel, and the density of the material is $7.801 * 10^{-6}$ kg/mm^3. The Young's modulus is $2.07 * 10^5$ N/mm^2, which means that

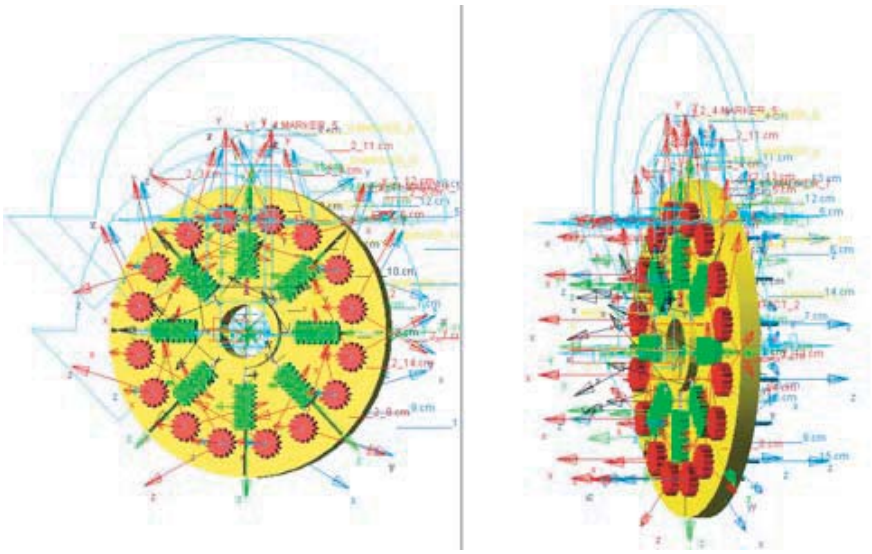

Figure 6. The virtual prototype model.

Table 2. The constraint relationship between the components of flux-adjusting device.

Constraint	Component 1	Component 2
Revolute joint	Disc	Ground
Translational joint	Sliding block	Disc
Revolute joint	Gear	Disc
Flexible connection	Sliding block	Disc
Contact	Sliding block	Gear

the steel has strong ability to resist deformation and can be regarded as a rigid body. The constraints conditions between the different components are shown in Table 2.

5. SIMULATION AND ANALYSIS OF DYNAMIC CHARACTERISTICS

5.1. The Motion Characteristics of Virtual Prototype

The time, type and step length should be set before the simulation calculation. According to the driving type of the mechanical flux-adjusting device, the relationship among rotational acceleration, speed and time can be obtained, as shown in Figure 7. From 0 to 1 sec, the virtual prototype model steadily accelerates to 5172 r/min with the acceleration of 310344.8 r/min^2 and decelerates to 0 with the acceleration of -310344.8 r/min^2 from 1 to 2 sec.

5.2. Analysis of Spring Deformation

For the given driving condition, the centrifugal forces of the sliding block under different rotational speeds are different. When the mechanical device is moving in a uniform circular motion, the tension is equal to the centrifugal force, and the direction is opposite. The deformation of spring provides the elastic tensile force of the sliding block, and the deformation length of the spring is equal to the displacement length of the sliding block. Therefore, the simulation analysis can be carried out by the variable of the spring. The calculation formula of the spring force is shown in Formula (3).

$$F = -k(r - r_0) - c\frac{dr}{dt} + f, \tag{3}$$

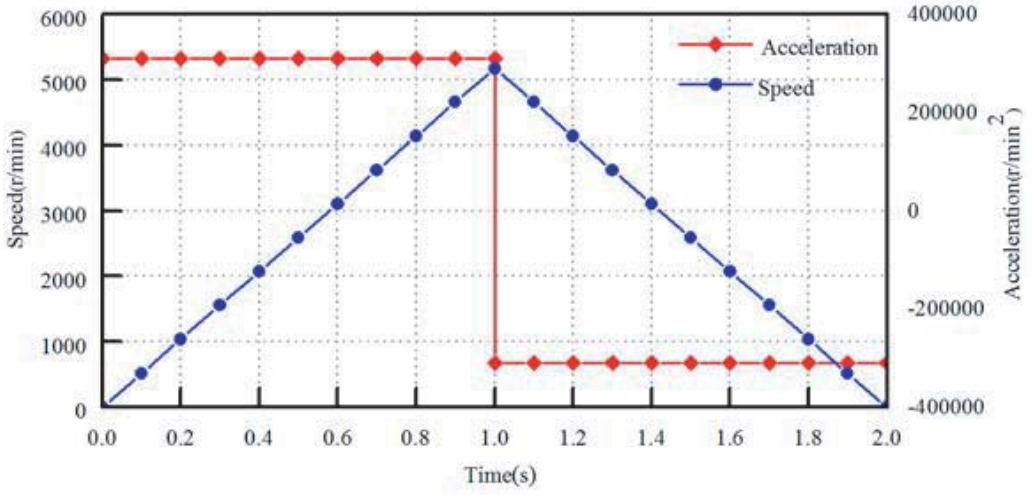

Figure 7. The relationship between acceleration and speed of virtual prototype.

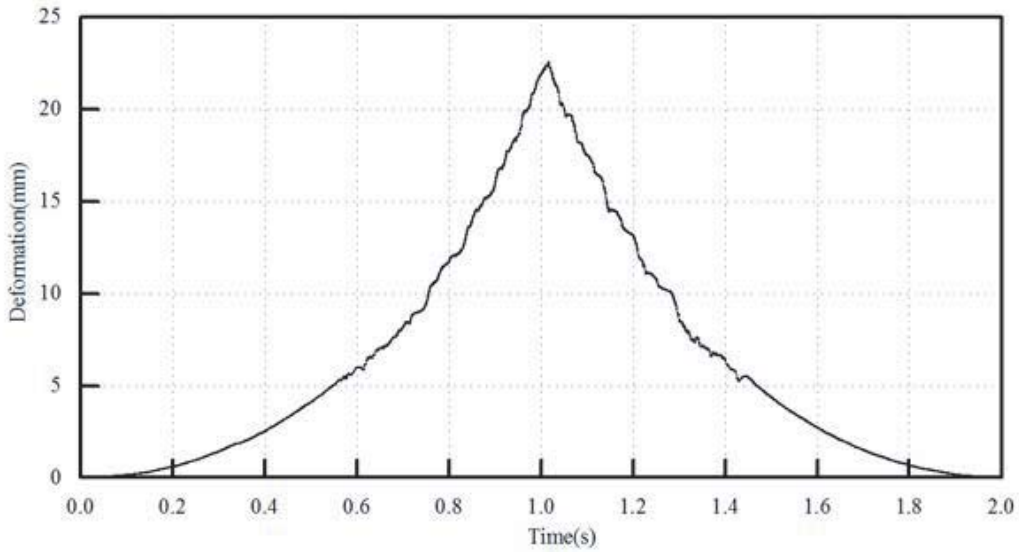

Figure 8. The deformation of the spring.

where k is the stiffness coefficient of spring, c the damping coefficient of spring, r_0 the initial length of spring, r the length of spring, and f the preload of spring.

The parameter of the spring is obtained by optimizing simulation. The spring stiffness coefficient is 0.2 N/mm, the damping coefficient 30 N · s/m, and the preload 0. The deformation of spring at different speeds is shown in Figure 8. The mechanical flux-adjusting device has the maximum speed at 1 second, while the spring has the maximum deformation of 22.5 mm after 1 second due to the damping coefficient of spring and the inertia of the sliding block. The length of sliding block is 25 mm, and that of the sliding chutes is 50 mm. The sliding block does not reach the limit position at the maximum speed, which can avoid the rigid collision at high speed due to the inertia effect.

5.3. The Rotation Angle of Gear

The cylindrical PMs and the gear rotate synchronously. Therefore, the main purpose of analyzing the mechanical flux-adjusting device is to obtain the rotation angle of the gear at different speeds.

When the device starts to rotate, gear follows the disc rotation synchronously, and the sliding block is not in contact with the gear. Because of rigid collision at high speed, there will be a fluctuating angle at the time of contact. As the speed increases, the gear rotates under the tangential force of the centrifugal sliding block, and the cylindrical PMs follow the rotation through the connecting rod. When the speed reaches the maximum, the rotation angle reaches the maximum value of 25 degrees. With the deceleration of the mechanical flux-adjusting device, the centrifugal force of the sliding block is reduced, and the rotation angle of the gear is reduced to 0 degrees. The auto-rotation angle of gear is shown in Figure 9.

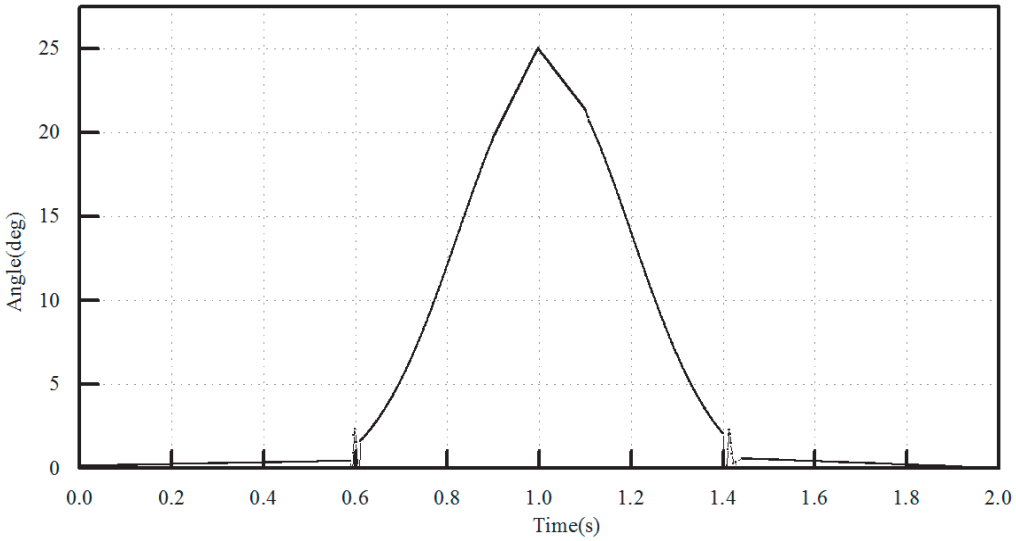

Figure 9. The auto-rotation angle of gear.

The mechanical flux-adjusting device has a better angle adjustment ability under appropriate spring parameters, which can realize continuous auto-rotation of the gear. The cylindrical PMs are rotated through the connecting rod drive, so the magnetization direction of PMs and the distribution of magnetic field are changed.

6. SIMULATION AND ANALYSIS OF ELECTROMAGNETIC PROPERTIES

6.1. The Distribution of Magnetic Field

The magnetic field distribution inside the machine is described by the vector magnetic potential A, and the fixed solution of the transient electromagnetic field can be described as Equation (4).

$$\frac{\partial}{\partial x}\left(\frac{1}{\mu}\frac{\partial A}{\partial x}\right)+\frac{\partial}{\partial y}\left(\frac{1}{\mu}\frac{\partial A}{\partial y}\right)=-\left(J_z-\sigma\frac{dA}{dt}\right), \tag{4}$$

where J_z is the conductivity current density, and $\sigma\frac{dA}{dt}$ is the eddy current density in magnetic field.

Equation (4) is discretized by FEM, and the function of the triangular element is used as the weighted integral. Then Equation (5) can be obtained.

$$\oiint\left(\{N\}^T\left[\frac{\partial}{\partial x}\left(\frac{1}{\mu}\frac{\partial A}{\partial x}\right)+\frac{\partial}{\partial y}\left(\frac{1}{\mu}\frac{\partial A}{\partial y}\right)\right]+\{N\}^T J_Z-\{N\}^T\sigma\frac{dA}{dt}\right)dxdy=0, \tag{5}$$

According to the design of the PMs, the magnetizing direction of the cylindrical PMs is radial below the base speed. The mechanical flux-adjusting device acts on the cylindrical PMs when the speed is above the base speed, which makes the PMs rotate and the magnetomotive force reduced, achieving the effect of flux-weakening. The distribution of the magnetic field at different speeds is shown in Figure 10. Figure 10(a) shows the magnetic field map below the base speed, and Figure 10(b) shows the

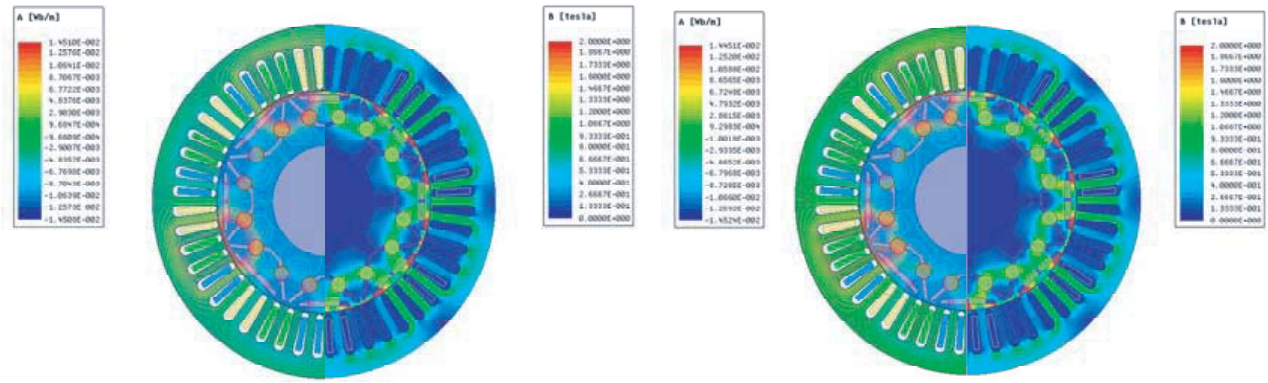

Figure 10. Magnetic field distribution diagram of machine. (a) Under basic speed. (b) Above basic speed.

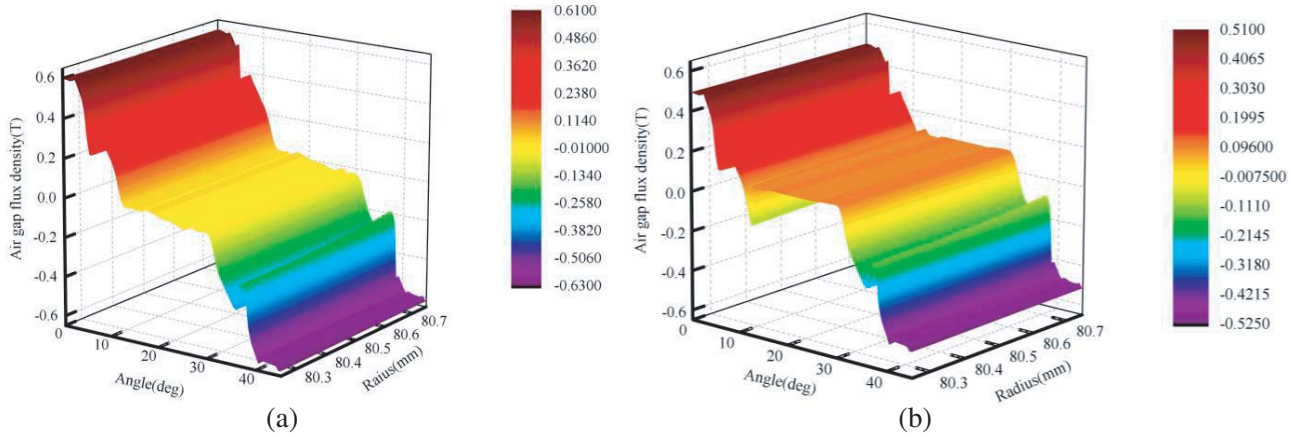

Figure 11. The 3D-MAP distribution of airgap flux density. (a) Under basic speed. (b) Above basic speed.

magnetic field distribution diagram above the base speed, using the same magnetic density distribution scale. The scale range is 0–2 T. According to the principle of minimum reluctance, the magnetic lines of flux are closed along the largest magnetic path of the magnetic conductance. When the magnetization direction of the PMs is changed, the reluctance increases in the d-axis, so the corresponding magnetic flux decreases. By comparison, the flux density of the stator core after the rotation of PMs is obviously lower than the flux density when the PMs are not rotating. Therefore, the magnetization direction of the cylindrical PMs and the distribution of the magnetic field can be changed.

6.2. Air Gap Flux Density

Neglecting the influence of the armature reaction and end winding, the air gap flux is only produced by PMs. For further studying the distribution of air gap magnetic density, different radii of airgap route are selected to calculate the airgap flux density. The 3D-map distribution is shown in Figure 11. It can be found that the air gap flux density near rotor is bigger than that near stator due to the magnetic resistance in the airgap, the magnet motive force is stored in airgap as energy, which leads to the decrease of flux-linkage. In other words, the larger the radius is, the smaller the airgap flux density will be. Because of the concentrated magnetic effect of IPMSM, the flux linkage in q-axis is almost nonexistent, and the flux density is 0. The maximum airgap flux density is 0.61 T when the ARPMMFVPMM operates under base speed, which is shown in Figure 11(a); however, when the

ARPMMFVPMM operates above base speed, the maximum airgap flux density is only 0.51 T. It is mainly due to the increase of the d-axis magnetic resistance after the cylindrical PMs rotate, causing more magnetic flux linkage. The larger the rotation angle of the PMs is, the smaller the air gap flux density is. It can be concluded that the magnetic flux density can be changed by rotating cylindrical PMs, so as to achieve the purpose of adjusting the magnetic field.

6.3. Winding Flux Linkage and EMF

The winding flux linkages when the cylindrical PMs are not rotating and rotate at 25 degrees are calculated by ANSYS. According to the mechanical dynamics simulation, the base speed is 3000 r/min, and the auto-rotation angle of the PMs is 25 degrees at the time of 4250 r/min. The calculation results are shown in Figure 12. Due to the auto-rotation of PMs, the peak of the winding flux will decrease. The magnetic flux of the armature winding can be effectively reduced by using mechanical flux-adjusting device.

The EMF of ARPMMFVPMM is calculated by Equation (6), according to the variation of the

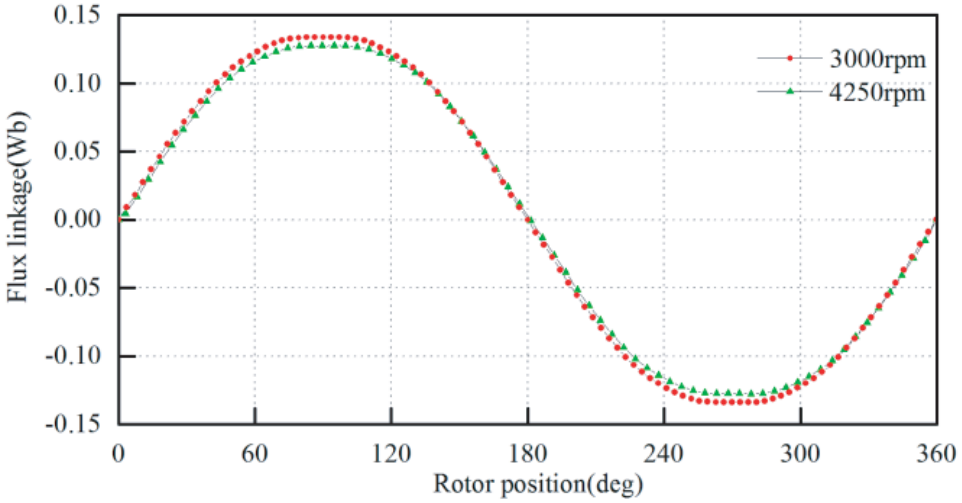

Figure 12. The flux linkage of ARPMMFVPMM.

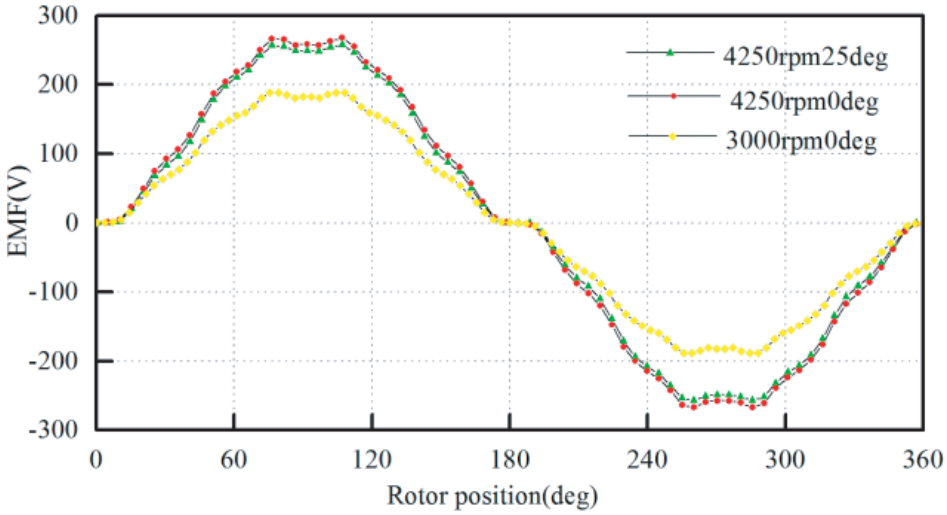

Figure 13. The induced EMF of ARPMMFVPMM.

phase winding flux linkage.

$$E = -\frac{d\Psi}{dt} = -N\frac{d\phi}{d\theta}\frac{d\theta}{dt} = -N\omega\frac{d\phi}{d\theta}, \tag{6}$$

where N is the winding turns per phase, ω the angle velocity of the rotor, and Ψ and ϕ are the phase winding flux linkage and magnetic flux of the phase coil, respectively. Figure 13 shows the induced EMF of the ARPMMFVPMM at different speeds.

When the IPMSM runs below the base speed, the EMF increases with the increase of speed. When the speed is 3000 r/min, the amplitude of the induction EMF is about 188 V, and when the speed reaches 4250 r/min, the amplitude of the EMF reaches 266 V. The magnitude of the EMF increases linearly with the speed, and the speed ratio is equal to the EMF ratio. While the mechanical flux-adjusting device acts on cylindrical PMs and the PMs are rotated a certain angle, the magnetic flux is reduced and the magnetic field distorted, so the EMF is changed. When the speed is up to 4250 r/min, the amplitude of the induction EMF is 250 V. The results show that the value of winding EMF can be effectively changed by adjusting the auto-rotation angle of the cylindrical PMs.

6.4. Flux Weakening Ability

ARPMMFVPMM is a kind of special motor based on the centrifugal force generated by the rotation of rotor. Its flux-adjusting ability is an important characteristic of this kind of motor. The change of the

Table 3. Flux Linkage and Weakening rate of ARPMMFVPMM.

Angle, deg	Flux linkage, 10^{-2} Wb	Weakening rate, %
0	13.39	0
25	13.08	2.3
50	12.77	4.6
75	11.12	16.9
100	8.35	37.6
125	5.69	57.5
150	3.73	72.1

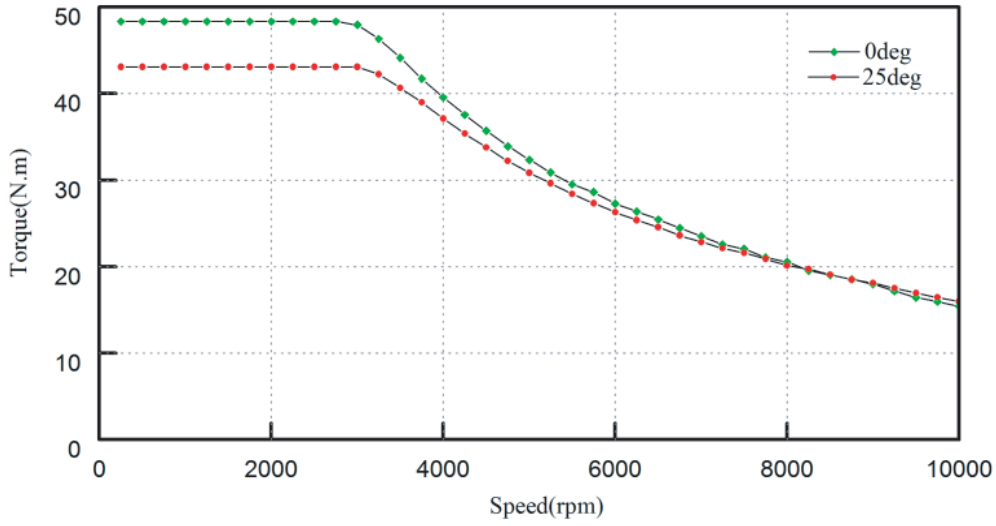

Figure 14. Torque-speed characteristics of ARPMMFVPMM.

magnetic field inside the machine will directly affect the change of the winding flux and no-load EMF. For obtaining the flux weakening ability in detail, the weakening rate is calculated when the cylindrical PMs are rotated at different angles, as shown in Table 3. It is obvious that the flux linkage will decrease as the rotation angle increases. After the rotation angle of the PMs exceeds 150 degrees, the air gap magnetic field distortion is serious, and the waveform is irregular. The limit values of voltage and current are limited by the maximum voltage and current of the DC side of the inverter, which affects the maximum torque and speed. Under the base speed, the PMSM is controlled by the maximum torque per Ampere (MTPA) to obtain the maximum torque. When the speed of the PMSM exceeds the base speed, the air gap magnetic field must be weakened because the EMF is constant. The flux weakening ability at the rated current is shown in Figure 14. When the cylindrical PMs are rotated 25 degrees, the maximum speed is significantly improved. So the ARPMMFVPMM has a better performance of flux weakening ability.

7. CONCLUSION

Aiming at the difficult problem of internal magnetic field adjustment of PM machines, a new type of ARPMMFVPMM is proposed, which uses an additional mechanical device to realize the magnetic field regulation. The following conclusions are obtained through the analysis of the principle of flux-adjusting, mechanical dynamic simulation and finite element calculation.

(1) The new mechanical flux-adjusting device can adjust the magnetization direction of cylindrical PMs in real time according to the change of the speed. Through the virtual prototype technology, the relationship between the spring deformation length and the rotation angle of the gear is obtained to verify the feasibility of the mechanical flux-adjusting device.

(2) The mechanical flux-adjusting IPMSM has good flux weakening capability. The electromagnetic characteristics under different states are analyzed, and the flux-weaken ability is obtained.

REFERENCES

1. Cheng, H., X. D. Liu, and J. Zhao, "Design and optimization of a high-band width low-speed high-torque permanent magnetic synchronous motor," *Transactions of China Electrotechnical Society*, Vol. 29, No. S1, 108–114, 2014.
2. Massimo, B., M. Giovanni, and B. Nicola, "Structural analysis of the interior PM rotor considering both static and fatigue loading," *IEEE Transactions on Industry Applications*, Vol. 50, No. 1, 253–260, 2014.
3. Liu, X. P., Y. Li, Z. Q. Liu, et al., "Optimized design of a high power density permanent magnet-assisted synchronous reluctance machine with low-cost ferrite magnets for EVs/HEVs," *COMPEL — The International Journal for Computation and Mathematics in Electrical and Electronic Engineering*, Vol. 35, No. 6, 1949–1964, 2016.
4. Wang, J., K. Zhao, and F. Chai, "Research review of flux-weakening of permanent magnet synchronous motor," *Micromotor*, Vol. 47, No. 01, 1–6+21, 2014.
5. Zhao, J. L., M. Y. Lin, X. H. Fu, et al., "Review and new progress of hybrid excitation synchronous motor and its control technology," *Transactions of China Electrotechnical Society*, Vol. 34, No. 33, 5876–5887, 2014.
6. Liu, X. P., A. H. Zheng, and C. Wang, "Design of a stator-separated axial flux-switching hybrid excitation synchronous machine," *International Conference on Electrical Machines and Systems (ICEMS)*, Vol. 1, No. 4, 1–4, 2011.
7. Liu, X. P., D. Cheng, M. Wang, et al., "Mechanical dynamic analysis and field-weakening capacity study of a variable magnetic flux axial magnetic permanent magnet motor," *Transactions of China Electrotechnical Society*, Vol. 23, 54–62, 2016.
8. Zhao, J., B. Li, and Z. X. Gu, "Research on an axial flux PMSM with radially sliding permanent magnets," *Energies*, Vol. 8, No. 3, 1663–1684, 2015.

9. Zhao, J., Y. S. Yan, Z. X. Gu, Z. Chen, and P. Zheng, "Research on an axial-axial flux compound-structure PMSM with varying air gap to fulfill field-weakening control," *Proceedings of the Electrical Machines and Systems*, Vol. 22–25, 3345–3349, 2014.
10. Tessarolo, A., M. Mezzarobba, and R. Menis, "A new rotor design for flux weakening capability improvement in spoke-type interior permanent magnet synchronous machines," *Proc. 9th Int. Conf. Ecol. Veh. Renew. Energies (EVER)*, 1–9, 2014.
11. Zhu, Z. Q., M. M. J. Al-Ani, X. Liu, M. Hasegawa, A. Pride, and R. Deodhar, "Comparison of flux weakening capability in alternative switched flux permanent magnet machines by mechanical adjusters," *Proc. 20th Int. Conf. Elect. Mach. (ICEM)*, 2889–2895, 2012.
12. Kim, K.-C., "A novel magnetic flux weakening method of permanent magnet synchronous motor for electric vehicles," *IEEE Trans. Magn.*, Vol. 48, No. 11, 4042–4045, 2012.
13. David, G. D., M. K. Andrew, E. Lyndon, and P. Mircea, "Analysis and design techniques applied to hybrid vehicle drive machines-assessment of alternative IPM and induction motor topologies," *IEEE Transactions on Industrial Electronics*, Vol. 59, No. 10, 3690–3699, 2012.
14. Cheng, L. X., Z. Y. Zhang, and R. Y. Tang, "A new structure for improving the field-weakening of the permanent magnet traction motor," *Transactions of China Electrotechnical Society*, Vol. 27, No. 03, 100–104, 2012.
15. Ling, H. Y., H. Yang, Y. K. Huang, and S. H. Fang, "Research review and new progress of memory motor," *Transactions of China Electrotechnical Society*, Vol. 33, No. 33, 57–67, 2013.
16. Liu, X. P., A. H. Zheng, and C. Wang, "Three dimensional finite element analysis and experimental study of a stator segmented axial flux switching hybrid excitation synchronous motor," *Transactions of China Electrotechnical Society*, Vol. 27, No. 10, 106–113, 2012.
17. Zhao, C. H., S. L. Ji, and X. W. Wang, "No-load characteristics of a rotor magnetic shunt radial structure hybrid excitation synchronous generator," *Transactions of China Electrotechnical Society*, Vol. 27, No. 09, 198–203, 2012.
18. Tessarolo, A., M. Mezzarobba, and R. Menis, "A novel interior permanent magnet motor design with a self-activated flux-weakening device for automotive applications," *International Conference on Electrical Machines(ICEM)*, 2603–2609, 2012.
19. Owen, R., Z. Q. Zhu, J. B. Wang, et al., "Mechanically adjusted variable-flux concept for switched-flux permanent-magnet machines," *2011 International Electrical Machines and Systems (ICEMS)*, 1–6, 2011.
20. Zhu, Z. Q., M. Al-Ani, X. Liu, et al., "Comparison of flux weakening capability in alternative switched flux permanent magnet machines by mechanical adjusters," *2012 XXth International Electrical Machines (ICEM)*, 2889–2895, 2012.
21. Tessarolo, A., M. Mezzarobba, and R. Menis, "A novel interior permanent magnet motor design with a self-activated flux-weakening device for automotive applications," *2012 XXth International Electrical Machines(ICEM)*, 2603–2609, 2012.
22. Chai, F., J. Ou, and Y. L. Pei, "Field-weakening research of double stator conical permanent magnet synchronous motor," *Transactions of China Electrotechnical Society*, Vol. 28, No. 7, 12–18, 2013.